Hunting the dark-Higgs: A search for a dark-Higgs boson in the $4b + p_{\mathrm{T}}^{\mathrm{miss}}$ final state at $\sqrt{s} = 13$ TeV with the ATLAS detector

Presented at the 32nd International Symposium on Lepton Photon Interactions at High Energies, Madison, Wisconsin, USA, August 25-29, 2025.

Thomas Dingley, on behalf of the ATLAS Collaboration.

ATL-PHYS-PROC-2025-113
21 November 2025

1 Introduction

A wealth of astrophysical evidence suggests the existence of dark matter (DM) in the universe [1–8]. Well-motivated particle DM candidates are weakly interacting massive particles (WIMPs): stable, electrically neutral particles whose weak-scale mass and couplings naturally reproduce the observed relic density via thermal freeze-out: a paradigm known as the *WIMP miracle* [9]. Given their weakly interacting nature, one typically looks for WIMP production in association with SM-reconstructed objects, such as jets, leptons or photons, with the WIMP DM candidate escaping detection. The presence of the invisible particle is thus inferred through the imbalance of transverse momentum in the event, defined as the negative vector sum of transverse momenta of all visible objects in the event ($p_{\mathrm{T}}^{\mathrm{miss}} = -\sum \vec{p}_{\mathrm{T}}$), leading to a signature of visible activity in association with $p_{\mathrm{T}}^{\mathrm{miss}}$. These are known as $X+p_{\mathrm{T}}^{\mathrm{miss}}$ signatures.

This note documents an analysis of LHC data collected during Run 2 (2015–2018) by the ATLAS collaboration searching for DM produced in association with a new scalar mediator decaying into a resonant pair of SM Higgs bosons, each subsequently decaying into $b\bar{b}$ — resulting in a $b\bar{b}b\bar{b} + p_{\mathrm{T}}^{\mathrm{miss}}$ final state [10].

A dark Higgs model is used to guide and optimise the search [11]. Motivated by the Higgs mechanism for electroweak symmetry breaking in the SM, this model explains massive fermionic dark matter (χ) through a similar mass generation mechanism in the dark sector, positing a dark Higgs boson, s. Such a weak-scale dark Higgs boson, interacting through mixing with the SM Higgs boson, will decay analogously to a SM Higgs boson of that mass. Thus the primary decays are into a pair of b-quarks at lower masses ($m_s < 150$ GeV), with diboson decays (WW, ZZ, hh) dominating at higher masses. An independent motivation for these models is an improved ability to reproduce the observed relic density [12], due to the presence of additional annihilation channels featuring the dark Higgs boson, such as $\chi\chi \to ss$, with subsequent decay of s into SM particles. This avoids the over-population common in simple or simplified models with weak-scale mediators [13].

The specific implementation of this model uses a two-mediator dark Higgs DM scenario, containing the dark Higgs boson, identified through its decay into hh, a new broken $U(1)'$ symmetry yielding an additional massive spin-1 Z' mediator, and a Majorana fermion DM candidate. The model parameters are the DM particle mass m_χ; the Z' mass $m_{Z'}$; the dark Higgs boson mass m_s; the Z' coupling with quarks g_q and with the DM candidate g_χ; and the mixing angle θ between the SM and dark Higgs bosons, which should be small to enable reproduction of the relic density and consistency with measurements of the Higgs boson. The dominant $q\bar{q} \to Z' \to s\chi\chi$ signal diagram for the large Z' masses explored in this note can be found in Figure 1.

Searches for the dark Higgs boson have been performed in the $b\bar{b}$ [14] and ZZ/WW fully hadronic [15] final states by the ATLAS collaboration, and the semi-leptonic WW final state by both the ATLAS and CMS collaborations [16, 17]. This note documents the first search in the $s \to hh \to 4b$ channel.

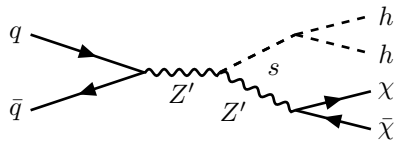

Fig. 1: Representative signal diagram for resonant $q\bar{q} \to Z' \to s\chi\chi$ production with the dark Higgs boson decay $s \to hh$.

2 Data and MC Simulated Samples

The analysis utilises the full 140 fb^{-1} of integrated luminosity collected from Run 2 of the LHC by the ATLAS experiment [18] at $\sqrt{s} = 13$ TeV. Unprescaled $p_{\mathrm{T}}^{\mathrm{miss}}$ triggers [19] are used to select events. An offline requirement of $p_{\mathrm{T}}^{\mathrm{miss}} > 200$ GeV, above the trigger thresholds (70–110 GeV), ensures the $p_{\mathrm{T}}^{\mathrm{miss}}$ sits well within the trigger plateau.

Signal samples of Monte Carlo (MC) simulated events are generated for 106 mass points covering a range of $m_{Z'}$ (420 GeV $< m_{Z'} <$ 3300 GeV) and m_s (250 GeV $< m_s <$ 435 GeV) values.

3 Event Selection

Hadronic jets are reconstructed from particle flow objects using the anti-k_t clustering algorithm with a radius parameter of $R = 0.4$ [20] and identified as originating from b-quarks using the `DL1r` [21] b-tagging algorithm at the 77% efficiency working point.

For signal, the final state b-jets are back-to-back in the transverse plane with $p_{\mathrm{T}}^{\mathrm{miss}}$ from the $Z' \to \chi\bar{\chi}$ decay. This kinematic handle enables various $p_{\mathrm{T}}^{\mathrm{miss}}$-based features to be utilised to improve signal background separation. The minimum transverse mass: $m_{\mathrm{T,min}}^{b}$, as defined in [10], is used for a system where a parent particle, X, decays into a b-jet and an invisible particle (or an object missed in reconstruction) and defines an upper-bound on the mass of the parent. The $t\bar{t}$ background is an example of this, in which $m_{\mathrm{T,min}}^{b}$ from $t \to bl\nu$, with the lepton missed in reconstruction, is bounded from above by m_t. Signal processes typically peak at higher $m_{\mathrm{T,min}}^{b}$ values.

Further cuts on the $p_{\mathrm{T}}^{\mathrm{miss}}$-significance [22] ($S(p_{\mathrm{T}}^{\mathrm{miss}}) > 7$) and on the minimum azimuthal angle between any of the jets and $p_{\mathrm{T}}^{\mathrm{miss}}$ in the final state ($\Delta\phi_{\mathrm{min}}^{4j} > 0.4$) are made, forming the full event preselection as defined in Table 1. The preselection eliminates the QCD background whilst significantly reducing the otherwise dominant $t\bar{t}$ background. The remaining backgrounds considered in the analysis are: Z+jets, $t\bar{t} + b\bar{b}$, $t\bar{t}+ \geq 1c$, $t\bar{t}+$ light, single top, W+jets, $t\bar{t} + X$ and diboson.

Table 1: Definition of the event preselection requirements, used to select the final states of interest [10].

Variable	Requirement
n_{leptons}	0
n_{jets}	$[4, 7]$
$n_{b\text{-jets}}$	≥ 3
$p_{\text{T}}^{\text{miss}}$ [GeV]	> 200
$\Delta\phi_{\text{min}}^{4j}$	> 0.4
$m_{\text{T,min}}^{b}$ [GeV]	> 80
$S(p_{\text{T}}^{\text{miss}})$	> 7
m_{T}^{4b} [GeV]	> 300

4 Higgs boson reconstruction and Machine Learning

Higgs boson candidates are reconstructed from b-jets in the final state. To avoid overly sculpting the background mass distributions towards the Higgs mass, an angular-based pairing minimising the maximal separation between b-jets is used, according to the metric:

$$\min(\Delta R_{\text{max}}(b, b)) = \min_{i,k,l,m}(\max(\Delta R(i, k), \Delta R(l, m))).$$

where, in the $4b$ region, i, k, l, m are the four b-jets and in the $3b$ region i, k, l correspond to b-jets and the fourth jet, m, chosen according to criterion outlined in [10].

The di-Higgs mass is a direct proxy for the dark Higgs mass. Any localised excess over the Standard Model expectation in the m_{hh} spectrum would point to a new resonance. Accordingly, the signal region (SR) is binned in m_{hh}. Moreover, this analysis greatly benefits from a neural network classifier to further enhance signal background separation. However, to not sculpt the background distribution towards signal-like m_{hh}-values, a modified loss-function is used. A feed-forward NN is implemented, where, in addition to a typical binary cross-entropy loss-function, L_{BCE}, a distance correlation [23, 24] term is included — penalising correlations between the NN output score and the di-Higgs invariant mass.

5 Statistics and Results

Backgrounds are estimated using a semi–data-driven approach in which MC predicts the shape and nominal yield, with fits to data in dedicated control regions (CRs) used to check and correct the modelling. CRs are designed to target the remaining dominant backgrounds of $t\bar{t}$ and Z+jets. A lower-bound on the NN-score of 0.35 is placed, together with the event preselection, to reject highly non-signal like background events. Then, a selection of $n_{b\text{-jets}} = 4$ defines `CR4b`, a region of 45% $t\bar{t}$+$b\bar{b}$-composition. Within the $3b$-region, a cut on $m_{\text{T,min}}^{b}$ of 200 GeV defines two further $t\bar{t}$ CRs: `CR3b-low` containing 57% $t\bar{t}$ + light, and `CR3b-high` comprised of similar amounts of Z+jets (25%), single top (20%) and $t\bar{t} + b\bar{b}$ (16%). The Z+jets CR is defined by relaxing the lepton veto and requiring two muons in the final state, with $p_{\text{T}}^{\text{miss}}$ reconstructed by assuming the muons to be invisible. A tight cut on the NN-score of 0.95 is used to define the SR, and, since the NN-classifier is decorrelated with the di-Higgs invariant mass, the SR is binned in m_{hh}. To define a validation region (VR), the NN-score cut

Table 2: Selections for all single top and $t\bar{t}$ CRs, the VR and SR [10].

Variable	Region requirement				
	`CR3b-low`	`CR3b-high`	`CR4b`	`VR`	`SR`
Preselection	pass			pass	pass
NN score	[0.35, 0.85)			[0.85, 0.95)	[0.95, 1.0]
$n_{b\text{-jets}}$	$= 3$	$= 3$	$= 4$	≥ 3	≥ 3
$m^{b}_{\mathrm{T,min}}$ [GeV]	[80, 200)	≥ 200	≥ 80	≥ 80	≥ 80

is loosened to $0.85 < \mathrm{NN} < 0.95$. An overview of all top CRs, together with the VR and SR, is given in Table 2.

The statistical interpretation of the search results is performed via simultaneous likelihood fits to the observed data, using the `HistFitter` framework [25].

For the background processes scaled by normalisation factors ($t\bar{t}$ + light, $t\bar{t} + b\bar{b}$, Z+jets), these appear as freely floating parameters multiplying the expected MC yields. A background-only fit is first performed to validate the SM background estimate. For this fit, only the four control region yields are included, and it is assumed that no signal is present. The fit constrains the values of the background normalisation factors, and the results of the fit are applied to the validation region, where agreement between the post-fit SM background and the observed data is checked, where a mild excess of 1.7σ is observed with no shape in the m_{hh}-distribution. The distribution of NN-scores is shown post background-only fit, together with the m_{hh} distribution in the SR, in Figures 2(a) and (b) respectively.

To place limits on the dark Higgs models at 95% CL using the CL_s method [26], the four CRs and the binned SR are fitted simultaneously. The parameter of interest in

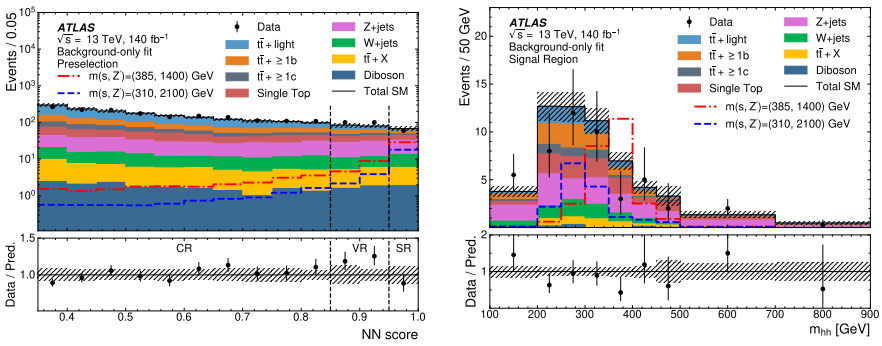

(a) (b)

Fig. 2: The observed data and expected background (a) NN score distribution after the preselection requirements and (b) m_{hh} distribution in the SR, after the background-only fit. The hashed bands show the total systematic and MC statistical uncertainty. Benchmark signal distributions are overlaid as dashed lines. The lower panel shows the ratio of data and predicted background yields [10].

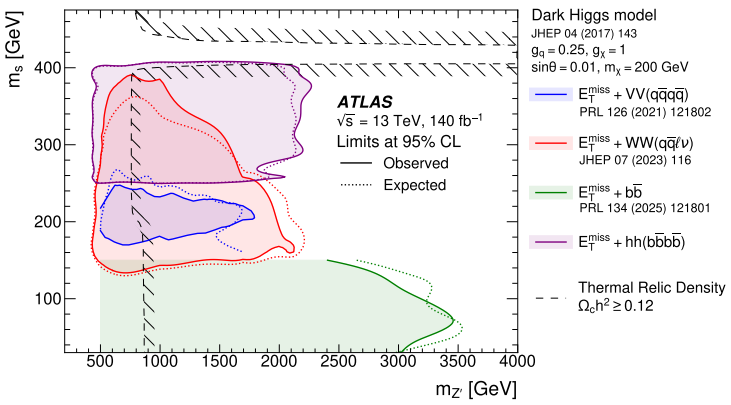

Fig. 3: A comparison of this analysis' exclusions with existent ATLAS searches [14–16]. Their observed and expected exclusion limits in the $(m_{Z'}, m_s)$ plane at 95% CL are shown. The observed relic density is indicated with a dashed line, with the diagonal lines indicating an overabundance of DM [10].

the fit is the signal strength, μ_{sig}, which multiplies the signal yield nominally predicted by the model. The observed and expected exclusion limits are calculated from the binned signal region, and shown alongside limits placed from other ATLAS dark Higgs boson searches in Figure 3. The observed limits follow the expectation closely, and are constrained by the large acceptance changes at the $Z' \to \chi\chi$ threshold of $m_{Z'} \sim 400$ GeV and the s-decay thresholds at $m_s \sim 250$ GeV and 400 GeV. At high $m_{Z'}$, the falling cross-section leads to a wider variation in the expected limits, and small fluctuations in the data result in slightly stronger or weaker exclusions than the median expectation accordingly.

6 Conclusions

A search for dark matter in a final state with significant $p_{\text{T}}^{\text{miss}}$ and a resonantly produced pair of Higgs bosons resulting in at least three b-tagged jets is performed, using the 140 fb^{-1} of Run 2 data recorded by the ATLAS detector at the LHC between 2015 and 2018. The observed data are found to be consistent with Standard Model predictions. The result is interpreted using a dark Higgs model, with a dark Higgs boson s giving rise to massive dark matter, and a Z' mediator. Upper limits are derived on the hypothesised particle masses for $250 < m_s < 400$ GeV, excluding Z' masses up to 2.3 TeV in a recommended model benchmark. This new signature significantly extends the constraints in this mass region existing from previous dark Higgs analyses by the ATLAS and CMS collaborations in different final states.

References

[1] E. Corbelli, P. Salucci, The Extended Rotation Curve and the Dark Matter Halo of M33. Mon. Not. Roy. Astron. Soc. **311**, 441–447 (2000). https://doi.org/10.1046/j.1365-8711.2000.03075.x. arXiv:astro-ph/9909252

[2] V.C. Rubin, et al., Rotational properties of 21 SC galaxies with a large range of luminosities and radii, from NGC 4605 (R=4kpc) to UGC 2885 (R=122kpc). Astrophysical Journal **238**, 471–487 (1980)

[3] K.G. Begeman, A.H. Broeils, R.H. Sanders, Extended rotation curves of spiral galaxies: Dark haloes and modified dynamics. MNRAS **249**, 523 (1991). https://doi.org/10.1093/mnras/249.3.523

[4] V. Trimble, Existence and nature of dark matter in the universe. Ann. Rev. Astron. Astrophys. **25**(1), 425–472 (1987). https://doi.org/10.1146/annurev.aa.25.090187.002233

[5] G. Bertone, D. Hooper, J. Silk, Particle dark matter: evidence, candidates and constraints. Phys. Rept. **405**(5-6), 279–390 (2005). https://doi.org/10.1016/j.physrep.2004.08.031

[6] J.L. Feng, Dark matter candidates from particle physics and methods of detection. Ann. Rev. Astron. Astrophys. **48**(1), 495–545 (2010). https://doi.org/10.1146/annurev-astro-082708-101659

[7] G. Hinshaw, et al., Nine-Year Wilkinson Microwave Anisotropy Probe (WMAP) Observations: Cosmological Parameter Results. Astrophys. J. Suppl. **208**, 19 (2013). https://doi.org/10.1088/0067-0049/208/2/19. arXiv:1212.5226 [astro-ph.CO]

[8] Planck Collaboration, Planck 2018 results. I. Overview and the cosmological legacy of Planck. Astron. Astrophys. **641**, A1 (2020). https://doi.org/10.1051/0004-6361/201833880. arXiv:1807.06205 [astro-ph.CO]

[9] G. Steigman, M.S. Turner, Cosmological Constraints on the Properties of Weakly Interacting Massive Particles. Nucl. Phys. B **253**, 375–386 (1985). https://doi.org/10.1016/0550-3213(85)90537-1

[10] ATLAS Collaboration, A search for dark matter produced in association with a dark Higgs boson decaying into a Higgs boson pair in $3b$ or $4b$ final states using pp collisions at $\sqrt{s} = 13$ TeV with the ATLAS detector. JHEP **09**, 067 (2025). https://doi.org/10.1007/JHEP09(2025)067. arXiv:2507.02175 [hep-ex]

[11] M. Duerr, A. Grohsjean, F. Kahlhoefer, B. Penning, K. Schmidt-Hoberg, C. Schwanenberger, Hunting the dark Higgs. JHEP **04**, 143 (2017). https://doi.org/10.1007/JHEP04(2017)143. arXiv:1701.08780 [hep-ph]

[12] Planck Collaboration, Planck 2018 results. VI. Cosmological parameters. Astron. Astrophys. **641**, A6 (2020). https://doi.org/10.1051/0004-6361/201833910. arXiv:1807.06209 [astro-ph.CO]

[13] ATLAS Collaboration, Constraints on simplified dark matter models involving an s-channel mediator with the ATLAS detector in pp collisions at $\sqrt{s} =$ 13 TeV. Eur. Phys. J. C **84**(10), 1102 (2024). https://doi.org/10.1140/epjc/s10052-024-13215-5. arXiv:2404.15930 [hep-ex]

[14] ATLAS Collaboration, Search for Dark Matter Produced in Association with a Dark Higgs boson in the $b\bar{b}$ Final State Using pp Collisions at $\sqrt{s} = 13\,\text{TeV}$ with the ATLAS Detector. Phys. Rev. Lett. **134**, 121801 (2025). https://doi.org/10.1103/PhysRevLett.134.121801. arXiv:2407.10549 [hep-ex]

[15] ATLAS Collaboration, Search for Dark Matter Produced in Association with a Dark Higgs Boson Decaying into $W^{\pm}W^{\mp}$ or ZZ in Fully Hadronic Final States from $\sqrt{s} = 13\,\text{TeV}$ pp Collisions Recorded with the ATLAS Detector. Phys. Rev. Lett. **126**, 121802 (2021). https://doi.org/10.1103/PhysRevLett.126.121802. arXiv:2010.06548 [hep-ex]

[16] ATLAS Collaboration, Search for dark matter produced in association with a dark Higgs boson decaying into W^+W^- in the one-lepton final state at $\sqrt{s} = 13\,\text{TeV}$ using $139\,\text{fb}^{-1}$ of pp collisions recorded with the ATLAS detector. JHEP **07**, 116 (2023). https://doi.org/10.1007/JHEP07(2023)116. arXiv:2211.07175 [hep-ex]

[17] CMS Collaboration, Search for dark matter particles in W^+W^- events with transverse momentum imbalance in proton–proton collisions at $\sqrt{s} = 13\,\text{TeV}$. JHEP **03**, 134 (2024). https://doi.org/10.1007/JHEP03(2024)134. arXiv:2310.12229 [hep-ex]

[18] ATLAS Collaboration, The ATLAS Experiment at the CERN Large Hadron Collider. JINST **3**, S08003 (2008). https://doi.org/10.1088/1748-0221/3/08/S08003 [hep-ex]

[19] ATLAS Collaboration, Performance of the missing transverse momentum triggers for the ATLAS detector during Run-2 data taking. JHEP **08**, 080 (2020). https://doi.org/10.1007/JHEP08(2020)080. arXiv:2005.09554 [hep-ex]

[20] M. Cacciari, G.P. Salam, G. Soyez, The anti-k_t jet clustering algorithm. JHEP **04**, 063 (2008). https://doi.org/10.1088/1126-6708/2008/04/063. arXiv:0802.1189 [hep-ph]

[21] ATLAS Collaboration, ATLAS flavour-tagging algorithms for the LHC Run 2 pp collision dataset. Eur. Phys. J. C **83**(7), 681 (2023). https://doi.org/10.1140/epjc/s10052-023-11699-1. arXiv:2211.16345 [physics.data-an]

[22] ATLAS Collaboration, The performance of missing transverse momentum reconstruction and its significance with the ATLAS detector using 140 fb^{-1} of $\sqrt{s}$ = 13 TeV pp collisions. Eur. Phys. J. C **85**, 606 (2025). https://doi.org/10.1140/epjc/s10052-025-14062-8. arXiv:2402.05858 [hep-ex]

[23] G.J. Székely, M.L. Rizzo, N.K. Bakirov, Measuring and testing dependence by correlation of distances. The Annals of Statistics **35**(6), 2769 – 2794 (2007). https://doi.org/10.1214/009053607000000505. URL https://doi.org/10.1214/009053607000000505

[24] G. Kasieczka, D. Shih, Robust Jet Classifiers through Distance Correlation. Phys. Rev. Lett. **125**(12), 122001 (2020). https://doi.org/10.1103/PhysRevLett.125.122001. arXiv:2001.05310 [hep-ph]

[25] M. Baak, G. Besjes, D. Côté, A. Koutsman, J. Lorenz, D. Short, HistFitter software framework for statistical data analysis. Eur. Phys. J. C **75**, 153 (2015). https://doi.org/10.1140/epjc/s10052-015-3327-7. arXiv:1410.1280 [hep-ex]

[26] A.L. Read, Presentation of search results: the CL_s technique. J. Phys. G **28**, 2693 (2002). https://doi.org/10.1088/0954-3899/28/10/313